STM JOURNALS
Scientific Technical Medical

Journal of Industrial Safety Engineering

Volume 1, Issue 1
www.stmjournals.com

Interference Effect between Prismatic Buildings Subjected to Microburst Wind

Kalyan Kumar Das*, Kalyan Prasad Sinhamahapatra, Amit Kumar Ghosh
Assam Engineering College, Guwahati, India
Department of Aerospace Engineering, IIT Kharagpur, India

Abstract

Severe thunderstorms are important weather phenomena which impact on various facets of national activity like civil and defense operation, particularly aviation, space vehicle launching and agriculture in addition to its damage potential to life and properties. One of the most important events in the thunderstorms is the "Downburst". Downbursts occur when a column of descending air reaches the ground and bursts out violently. This downward motion abruptly changes direction and produces a peak wind speed close to the ground. A synoptic, or atmospheric boundary layer (ABL) wind however does not reach its maximum wind speed until much higher above the earth's surface. It is believed that downburst is generated when the moist buoyant air moving upward can no longer be sustained above and subsides into downdraft. Downbursts can be wet (accompanying rain) or dry and are further classified as either microburst or macroburst depending on their horizontal extent of damage. In India severe thunderstorms over the Gangetic West Bengal and Assam, known as "Kalbaishakhi" and "Bordoisila" respectively are very much destructive. In this work an attempt has been made to simulate the dry downburst wind numerically using the impinging jet model of the downburst. A CFD code is developed for the numerical simulation based on the vorticity-vector potential approach using a Large Eddy Simulation (LES) technique for the turbulence. The primary objectives of the present work are to investigate the flow dynamics of the downburst wind and its effect on prismatic buildings. The numerical results generated for the downburst wind profile are compared with the experimental results obtained from the physical microburst simulator developed by the authors with a 500 mm diameter jet and also with the available full scale data. Very good agreement is observed.

Keywords: *prismatic buildings, wind speed, downburst, thunderstorms*

****Author for Correspondence*** E-mail: kkdas1971@gmail.com

INTRODUCTION

Thunderstorms have always impressed humans and the cumulonimbus cloud is still one of the most visually striking and photogenic of all natural phenomena. However many hazardous weather are associated with thunderstorms. Lightning causes many fires around the world each year and leads to severe injuries or death. Thunderstorms can cause intense rainfall, which can lead to flash flooding and hail larger than a tennis ball. Strong winds associated with thunderstorms can knock down trees and power houses. Severe thunderstorms are responsible for large amount of wind induced damage around the globe. Unlike large and continental cyclones, severe local storms intensify very rapidly and dissipate after causing damage. The worst severe local storm is the tornado, which is characterized by fast rotating column of rising air which originates on or near the ground where the air swirls and converges at high speed. The downburst is the anti-tornadic storm characterized by slow rotating column of descending air, which bursts out violently after reaching the ground. The scale and suddenness of a downburst makes it a great danger to aircraft, particularly those at low altitude or are taking off or landing. There are two types of downbursts: wet, which accompanies rain and dry. Fujita (1985) further subdivided downbursts into "microburst", "with damaging wind extending

4 km or less", and "macroburst" with "outburst wind extending more than 4 km in the horizontal direction" [1].

With computational fluid dynamics (CFD), it is possible to simulate complex wind events and it is relatively easy to alter inlet, outlet and surface conditions. CFD also allows calculations to be made for the influence of various geometric structures on a flow field. The major problem associated with CFD simulation is accurate modelling of the turbulence in the wind as there is little physical data for the turbulence within a true microburst. Physical modelling too has several advantages and disadvantages. One of the major advantages of the physical modelling is the fact that air itself is used for experimentation. This helps to minimize errors, caused due to incorrect modelling of test fluids. Modelling with air as the test fluid has produced relatively good representation of the full scale phenomenon. However, it is very difficult to model the true downburst due to the complexity of the event.

The primary objective of this study is to simulate dry downburst numerically by using the impinging jet model. To achieve this objective three-dimensional CFD code is developed that can predict the wind field for different input parameters like cloud height (jet separation), jet diameter, downdraft speed (Reynolds number). Effects of downburst wind on prismatic buildings have been investigated.

MATHEMATICAL MODEL

In this work the 3D modelling of the downburst is accomplished using the vorticity-vector potential formulation. The 3D incompressible space-averaged Navier-Stokes equations in vorticity-vector potential formulation, neglecting the second order terms, are as follows,

$$\frac{\partial \xi_x}{\partial t}+\frac{\partial(u\xi_x)}{\partial x}+\frac{\partial(v\xi_x)}{\partial y}+\frac{\partial(w\xi_x)}{\partial z}-\xi_x\frac{\partial u}{\partial x}-\xi_y\frac{\partial u}{\partial y}-\xi_z\frac{\partial u}{\partial z}-\frac{1}{Re}\nabla^2\left(\frac{\upsilon+\upsilon_{sgs}}{\upsilon}\right)\xi_x=0 \quad (1a)$$

$$\frac{\partial \xi_y}{\partial t}+\frac{\partial(u\xi_y)}{\partial x}+\frac{\partial(v\xi_y)}{\partial y}+\frac{\partial(w\xi_y)}{\partial z}-\xi_x\frac{\partial v}{\partial x}-\xi_y\frac{\partial v}{\partial y}-\xi_z\frac{\partial v}{\partial z}-\frac{1}{Re}\nabla^2\left(\frac{\upsilon+\upsilon_{sgs}}{\upsilon}\right)\xi_y=0 \quad (1b)$$

$$\frac{\partial \xi_z}{\partial t}+\frac{\partial(u\xi_z)}{\partial x}+\frac{\partial(v\xi_z)}{\partial y}+\frac{\partial(w\xi_z)}{\partial z}-\xi_z\frac{\partial w}{\partial x}-\xi_z\frac{\partial w}{\partial y}-\xi_z\frac{\partial w}{\partial z}-\frac{1}{Re}\nabla^2\left(\frac{\upsilon+\upsilon_{sgs}}{\upsilon}\right)\xi_z=0 \quad (1c)$$

$$\upsilon_{sgs}=(C_s\Delta)^2[\tfrac{1}{2}S_{ij}]^{\frac{1}{2}};\ \ \Delta=(\Delta x\Delta y\Delta z)^{\frac{1}{3}};\ \ S_{ij}=\tfrac{1}{2}(\frac{\partial u_i}{\partial x_j}+\frac{\partial u_j}{\partial x_i})$$

The vector Poisson's equation for the 3D flow is

$$\xi=-\nabla^2\psi \quad (2)$$

From the equation 4.26 and the continuity equation following Poisson's equations can be derived

$$\nabla^2 u=-\frac{\partial \xi_y}{\partial z}+\frac{\partial \xi_z}{\partial y} \quad (3a) \qquad \nabla^2 v=-\frac{\partial \xi_z}{\partial x}+\frac{\partial \xi_x}{\partial z} \quad (3b)$$

$$\nabla^2 w=-\frac{\partial \xi_x}{\partial y}+\frac{\partial \xi_y}{\partial z} \quad (3c)$$

$$u=\frac{\partial \psi_z}{\partial y}-\frac{\partial \psi_y}{\partial z} \quad (4a)$$

$$v=\frac{\partial \psi_x}{\partial z}-\frac{\partial \psi_z}{\partial x} \quad (4b)$$

$$w=\frac{\partial \psi_y}{\partial x}-\frac{\partial \psi_x}{\partial y} \quad (4c)$$

The resolved vorticity transport equations 1 are normalized with the jet velocity and diameter. The vorticity transport equation 1 is solved by an explicit time-marching technique. As an alternative to solving three Poisson's equation for the ψ, the three Poisson's equation for the resolved velocity components (equations 3a, 3b and 3c) are solved directly using a successive over-relaxation technique. Details of the numerical method are given in the subsequent sections. The density and molecular viscosity of air are taken as 1.225 kg/m^3 and 1.7894×10^{-5} N-sec/m^2 for the present numerical simulations. The Smagorinsky constant (C_s) is taken as 0.18. It is further assumed that the flow enters the computational domain with the jet exit velocity where the fluid is stationary at t = 0. The size of the computational domain selected is $12D_{jet} \times 8D_{jet} \times 12D_{jet}$ in the x, y and z directions respectively.

No-slip boundary condition is imposed on the impinging plate. The gradients of all parameters are equated to zero at the outflow boundaries and the free slip condition is imposed on the jet walls. At the inlet boundary the velocity is assumed to be axial and in the negative z direction. In addition, an anticlockwise vorticity of ξ_z =0.1 rad/s is assumed at the inlet for a swirling jet. The symmetric boundary condition is applied along the jet axis. The boundary conditions at the no-slip boundary are tricky. The ψ components are not all zero, rather the components tangential to the surface are zero and the normal derivative of the normal component is zero [2].For a wall on the *xz* plane

$$\xi_x = 0$$

$$\xi_y = -\frac{\partial w}{\partial z}$$

$$\xi_z = +\frac{\partial v}{\partial x}$$

The wall vorticity components can be directly computed from the above equations [2]

$$\xi(ia,j,k) = -\frac{\partial w}{\partial x}\Big|_{ia,j,k} = -\left[\frac{4w(ia+1,j,k)-w(ia+2,j,k)}{2\Delta x}\right] \quad (5)$$

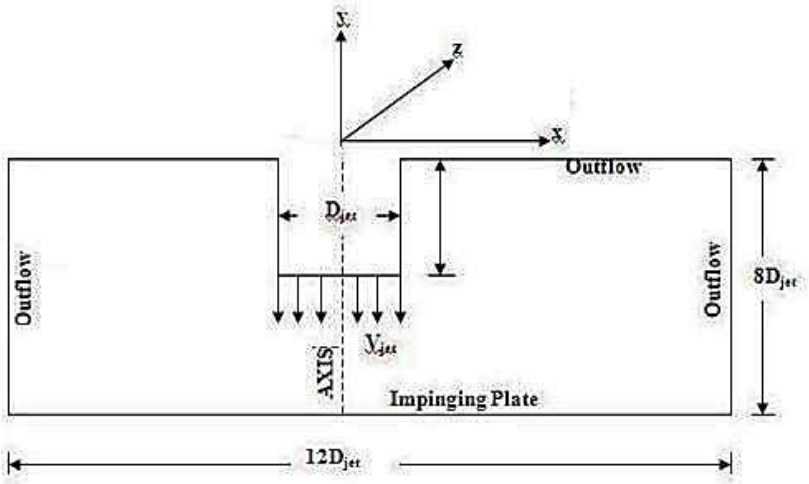

Fig. 1: *Computational Domain for the 3D Simulation (sectional view).*

A grid dependency study is made initially to verify the algorithm and the code. The computed results using two grids 180 × 120 × 180 and 270 × 180 × 270 for the flow at Reynolds number 1.1×10^5 and H/D_{jet} = 1.5 at radial distance of D_{jet}. No significant change in the radial velocity profile is observed in the solutions on the two grids. Similar comparisons are found in other cases as well. Consequently the grid with the resolution 180 × 120 × 180 is adopted for all subsequent computations.

RESULTS AND DISCUSSION

Figure 2(a) and (b) show the resolved vorticity fields in the numerically simulated downburst at non-dimensional time instant of 1.0 at a Reynolds number of 1.1×10^5 for H/D_{jet}=1.0 and 1.5 respectively. The formation of the primary, secondary and tertiary vortices in the

wall jet region is clearly observed in the vorticity fields presented in these figures. Numerous other eddies are also seen in these figures. Tertiary vortex is more visible when the jet is closer to the ground i.e. for a lower value of H/D_{jet}. Five distinct major vortices are observed within the downburst flow field: a primary, an intermediate, a trailing, a counter-rotating secondary and a tertiary vortex as seen in Figure 2(a).

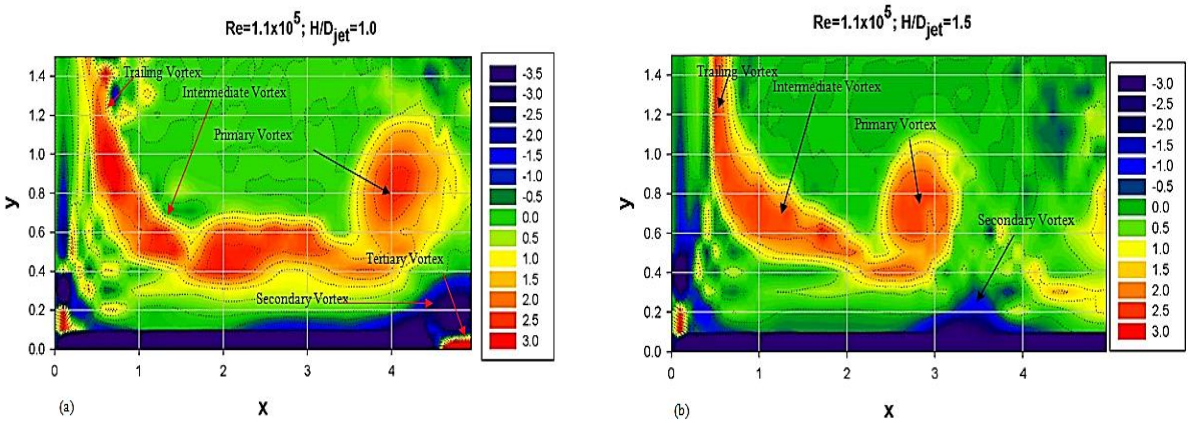

Fig. 2: *Resolved Vorticity Fields at $Re=1.1\times10^5$ for $H/D_{jet}=1.0$ and 1.5 at Time 1.0*

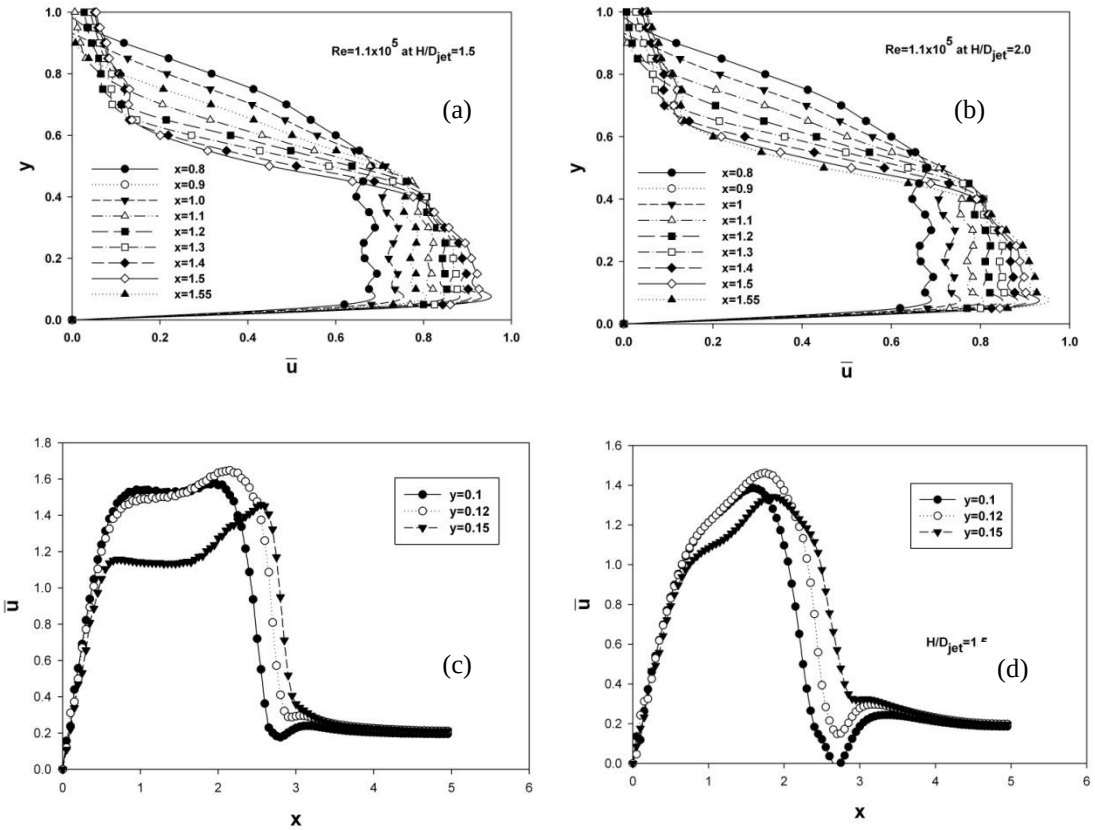

Fig. 3: *Time Averaged Radial Velocity ($\bar{u}$) Profiles at Different Locations.*

Figure 3(a) shows the time averaged radial velocity ($\bar{u}$) profiles at different radial locations at the Reynolds number of 2.2×10^5 and H/D_{jet} ratio of 1.5 at non-dimensional time 1.0. The figure shows that the time averaged radial velocity ($\bar{u}$) is highest at about $1.2<x<1.4$ and close to the ground. The vertical location of the maximum velocity is at y=0.05 – 0.07 for almost all radial locations. Figure 3(b) presents the variation in radial velocity along radial direction at the Reynolds number of 2.2×10^5 and H/D_{jet} ratio of 2.0 at

non-dimensional time 1.0. Here also it is seen that maximum time averaged radial velocity occurs in the range $1.2<x<1.5$. The vertical location of the maximum velocity is at $y=0.05 - 0.07$ for almost all radial locations. Similar results can be seen for other Reynolds number and jet separation as well. Very high decay of radial velocity with height can be seen for higher values of x. This can be attributed to the presence of strong counter rotating secondary vortex in the flow field. Figure 3(c-d) show the variation of time averaged radial velocity ($\bar{u}$) in the radial direction (x) at different heights (y=0.1, 0.12 and 0.15) for different Reynolds numbers and jet separations. From these figures it can be concluded that the radial location of the maximum radial velocity at almost all heights depends on the jet separation (H/D_{jet}). It is seen that the location of the maximum time-averaged radial velocity moves closer to the downburst axis for higher value of H/D_{jet}. Frequency (ω) spectra of u^2 are presented in figure 4(a) and (b) for the Reynolds number 1.1×10^5 at two radial locations (x=1.0 and1.3) at elevations y=0.03 (half of the Eaves height), y=0.059 (Eaves height) and y=0.12. These heights are chosen as maximum velocity occurs in that region. Frequencies higher than 200 Hz are not shown in the spectra as the energy at those frequencies are much smaller. Most of the energy at the reference locations is contained at lower frequencies. The spectra also indicate the nature of turbulence and the scales resolved in the simulation. The spectra at the three locations clearly show the presence of wider spectrum of eddies at x=1.3 and 1.4 compared to x=1.0 suggesting more intense turbulence at x=1.3 and 1.4.

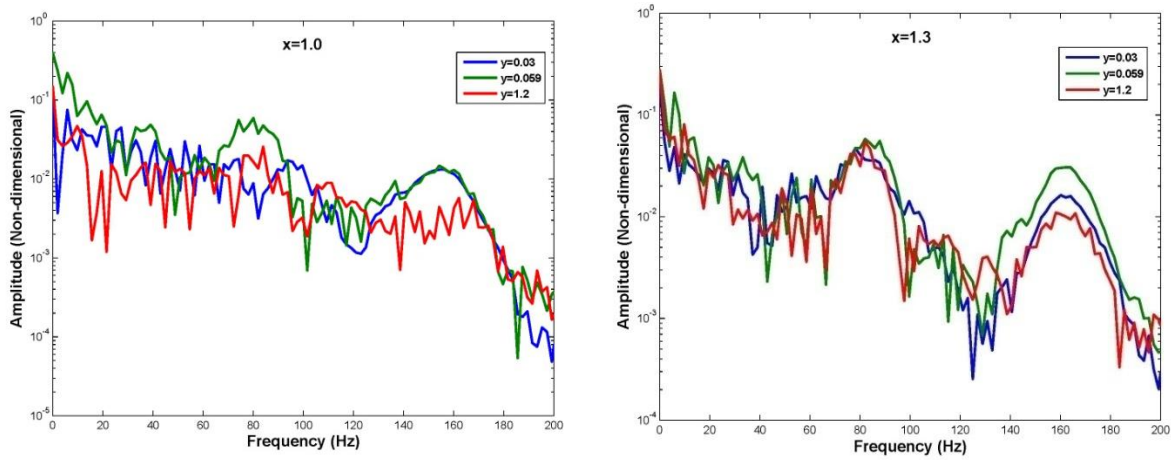

(a) (b)

Fig. 4: *Frequency Spectrum of u^2 at Reynolds Number 1.1×10^5*

In order to investigate the second order statistics, radial profiles of the turbulence intensity within the range of x = 0.8 – 1.2 at Reynolds number 1.1×10^5 at H/D_{jet}=1.0 and 1.5 are presented in figure 5(a) and (b). At H/D_{jet}=1.0 nearly identical turbulence intensity profiles are observed at x = 0.8 and 1.0 with small differences in intensity levels but the turbulence intensity profiles at x = 1.2 are different as the primary vortex gains momentum in the radial direction beyond x = 1.1. The turbulence levels at x = 1.2 are considerably higher compared to the other two locations. At the higher plate separation of H/D_{jet}=1.5 the turbulence intensity is found to be little lower. The difference in intensity levels at the three locations is also reduced due to decrease in intensity at x = 1.2 and increase in intensity at the other two locations.

The computed and experimental mean radial velocity profiles from the present simulations are compared with the field observation data from the project NIMROD [3] and empirical profiles discussed in Refs. [4] and [5]. The comparison is presented in Figure 6(a). The radial velocity in the figure is normalized with the maximum radial velocity and the height is normalized with respect to the height at which radial velocity falls to 50% of the maximum.

The experimental and numerical results shown in figure 6(a) are for jet velocity 30 m/s and H/D_{jet} =1.0. The computed time-averaged radial velocity profile matches closely with the experimental data as well as the field data. The two-dimensional computation too agrees reasonably well. Very good agreement is also observed with the full scale data from NIMROD [2].Figure 6(b) shows the measured and computed radial velocity at a height of $0.1D_{jet}$ from the test surface for the configuration having H/D_{jet} = 1.0 (R_1) and jet velocity of 10 m/s (V_1), which corresponds to a Reynolds number of 1.1×10^5. The results are compared with the well-known correlation proposed by Holmes and Oliver (2000).

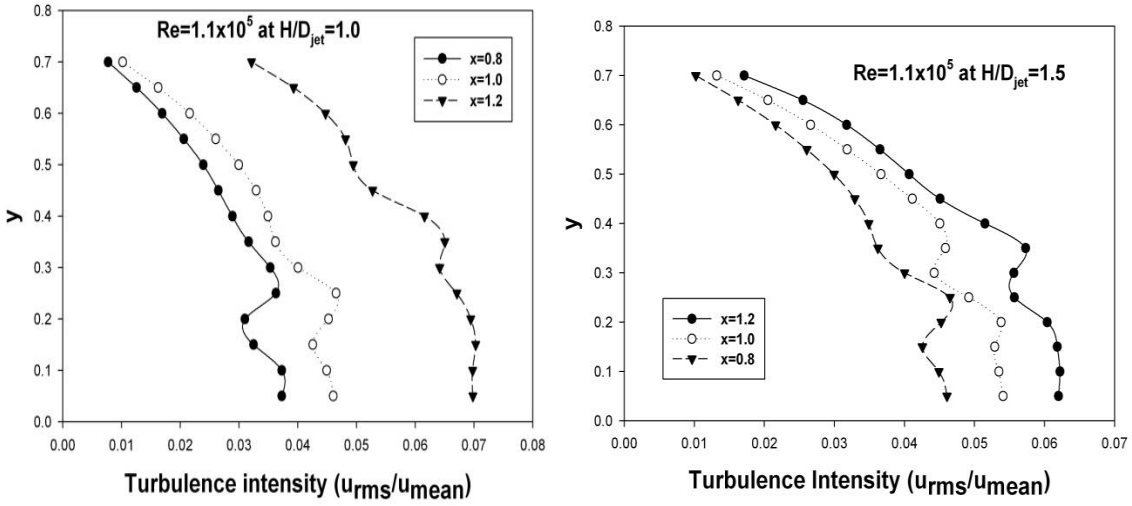

(a) (b)

Fig. 5: *Radial Turbulence Intensity Profiles at Reynolds Number 1.1×10^5*

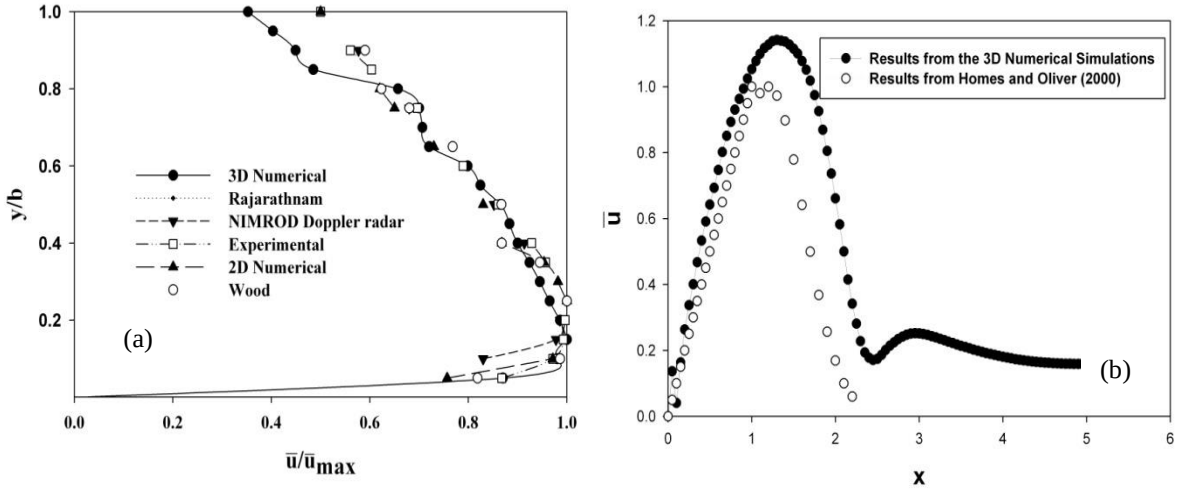

Fig. 6: *Comparison with Full Scale Data.*

Figure 7(a) shows the streamline plot for flow over three prismatic buildings in tandem arrangement. Figure (c-e) shows the coefficient of pressure distribution over the buildings. Figure 7(b) shows the grid distribution around the buildings. Figure 8 (a) shows the streamline plot for flow over two buildings and 8(b) shows the grid around the buildings. Figure 8 (c–d) shows the C_p distribution over upstream and downstream buildings.

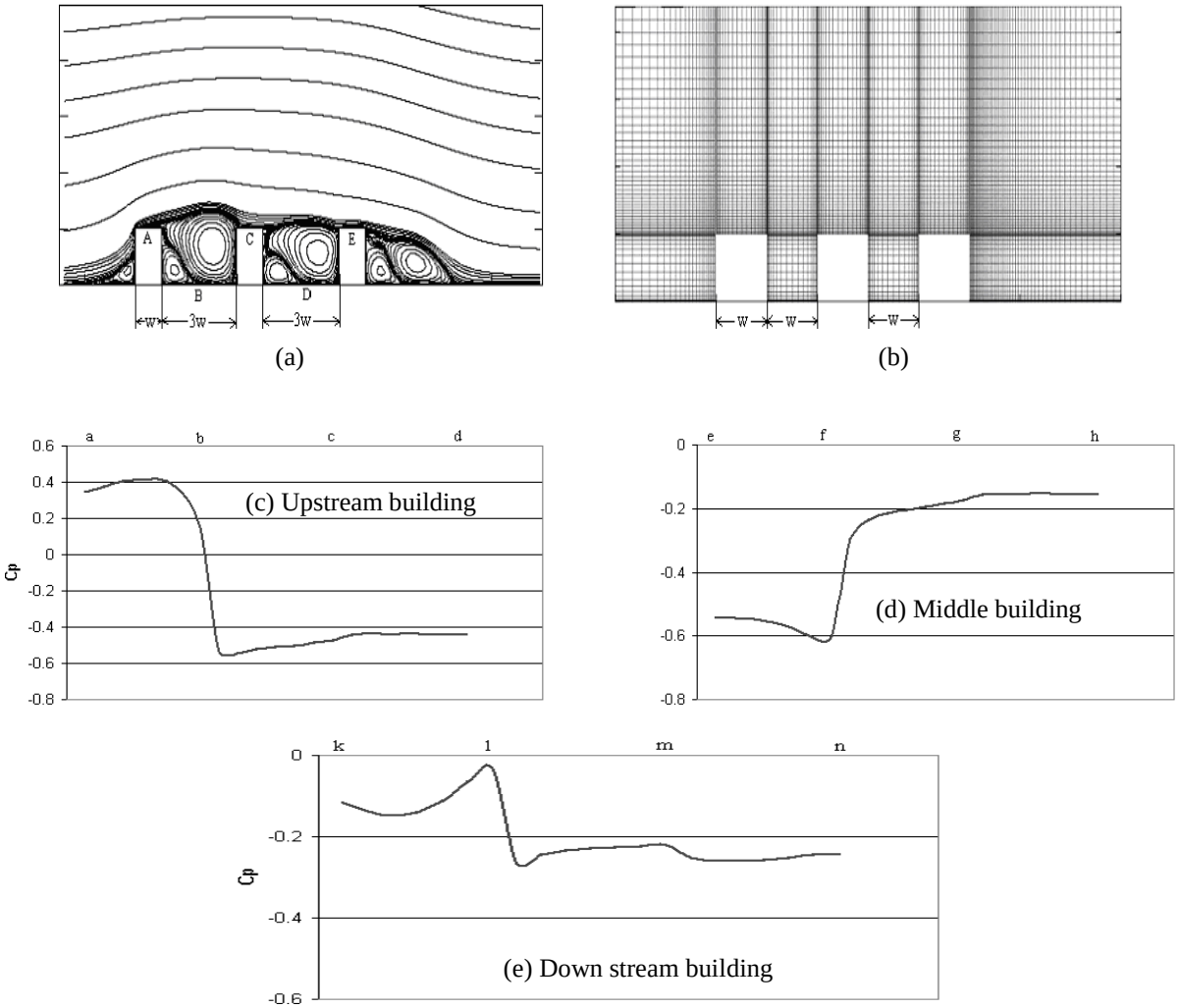

Fig. 7: *Flow over Three Prismatic Buildings of Equal Height, Height/Width 1.0, Spacing 3w.*

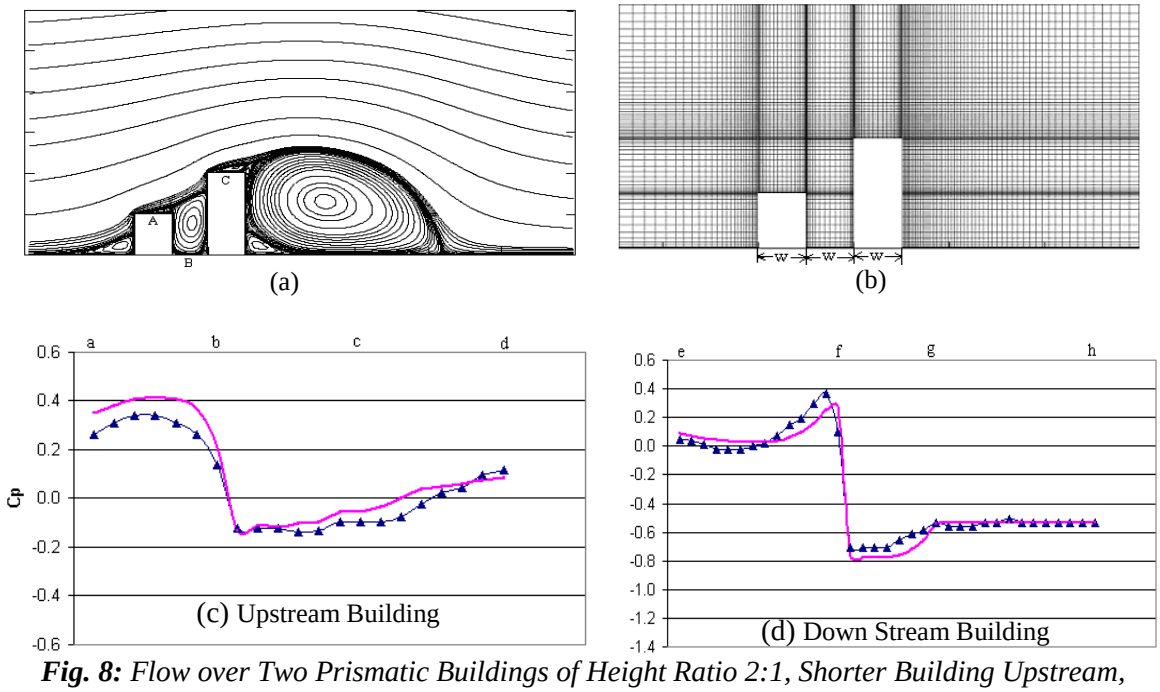

Fig. 8: *Flow over Two Prismatic Buildings of Height Ratio 2:1, Shorter Building Upstream, Spacing 1 w.*

CONCLUSIONS

A 3D large eddy simulation based CFD code is developed using the vorticity-vector potential approach to simulate the dry downburst numerically. Both resolved and time-averaged velocity, vorticity and pressure profiles are investigated for various Reynolds numbers and jet separations. Results obtained from the experimental and numerical simulations are compared with full scale data of NIMROD Doppler radar [3] and empirical results in Refs. [4–7].The present study reveals the following facts regarding the downburst flow field,

i. Five distinct vortices coexist in the simulated downburst flow field along with numerous smaller eddies. The trailing and intermediate vortices form before the jet impact and the primary, secondary and tertiary vortices form after the impact of the jet in the wall jet region. Several transient vortices form near the test surface immediately after the jet impact which produces tremendous wind shear near the ground.
ii. Separation and reattachment of the transient vortices strengthen the primary vortex near the ground and produces high velocity near the ground. The maximum velocity occurs at about 5 – 7% of D_{jet} above the ground and about $1.5D_{jet}$ away from the jet axis. The primary vortex core (which will indicate very high wind shear) is located closer to the jet axis for lower Reynolds number and also its location is nearer to the impinging surface at lower Reynolds number. Reynolds number dependency of the simulated downburst flow may be attributed to the unsteady separation of the boundary layer.
iii. The radial location of the maximum radial velocity is closer to the jet axis for higher value of H/D_{jet} but the axial location of the maximum radial velocity is almost independent of Reynolds number and jet separation (H/D_{jet}).
iv. For two buildings of identical height spaced one building width apart, flow circulates within the gap between the buildings and a vortex develops. The shear layer originating at the windward corner of the upstream building extends downstream and reattaches at a point behind the downstream building. As the spacing increases, the shear layer becomes curved, the vortex in the gap stretches horizontally and a secondary vortex starts developing at the base of the leeward face of the upstream building. Further the present study shows that as the gap between the buildings increases the large vortex on the leeward face of the downstream building starts moving further downstream and as a result the reattachment point of the shear layer also starts shifting downstream. When the height of the two buildings is doubled, only vortices get stretched in the vertical direction without any change in the general flow structure.
v. When a short building is placed upstream of a tall building(twice the height of the short building) with spacing one building width, the study shows that the shear layer that forms at windward corner of the short building hits the windward face of the tall building near the top corner. At the same time another shear layer originates at the windward sharp corner of the tall building which reattaches at some point downstream behind the tall building. As usual the flow circulation in the form of a vortex occurs in the gap between the buildings and a large vortex bounded by shear layer exists on the leeward face of the tall building.
vi. Study on three buildings in tandem has been made for four typical cases. As expected the flow pattern of the middle building is influenced by the presence of the upstream and downstream buildings. Vortices develop on either side (windward and leeward) of the central building. The size of the vortices is equal when the buildings are of identical height. If a short building is placed at the centre with two tall buildings on either side the flow pattern on this building is dominated by vortices all around including the roof. The effect of increasing spacing between the buildings is to stretch the vortices horizontally and to promote the growth of secondary vortices at the base.

REFERENCES

1. Fujita T.T., Downburst: Microburst and Macroburst, *Univ. of Chicago Press*, Chicago, Illinois. 1985.
2. Roache P.J, Computational Fluid Dynamics, *Hermosa Publishers*.1976.
3. Fujita T.T., Tornadoes and downbursts in the context of generalized planetary scales. *J. Atmos. Sci.* 1985; 38: 1511–1534p.
4. Rajaratnam N., Turbulent Jets, *Elsevier Scientific Publishing Company*, Amsterdam.1976.
5. Wood G.S., Kwok K.C.S., Motteram, N.A. and Fletcher, D.F., Physical and Numerical Modeling of Thunderstorm Downbursts, *Wind Engineering and Industrial Aerodynamics*, 2001; 89: 535–552p.
6. Holmes J.D., Oliver S.E., An empirical model of a downburst, *Eng. Structure.* 2000; 22: 1167–1172p.
7. Hjelmfelt M.R., 1988, Structure and life cycle of microburst outflows observed in *Colorado. J. Appl. Met.* 27; 1988: 900–927p.